Cell Stem Cell
Resource

Epigenomic Profiling of Young and Aged HSCs Reveals Concerted Changes during Aging that Reinforce Self-Renewal

Deqiang Sun,[2,9] Min Luo,[1,9] Mira Jeong,[1,9] Benjamin Rodriguez,[2] Zheng Xia,[2] Rebecca Hannah,[3] Hui Wang,[4] Thuc Le,[5] Kym F. Faull,[5] Rui Chen,[4] Hongcang Gu,[7] Christoph Bock,[7,8,11] Alexander Meissner,[7] Berthold Göttgens,[3] Gretchen J. Darlington,[6,10] Wei Li,[2,10,*] and Margaret A. Goodell[1,2,10,*]

[1]Stem Cells and Regenerative Medicine Center, Department of Pediatrics and Molecular and Human Genetics, Baylor College of Medicine, One Baylor Plaza, Houston, TX 77030, USA
[2]Dan L. Duncan Cancer Center and Department of Molecular and Cellular Biology, Baylor College of Medicine, Houston, TX 77030, USA
[3]Department of Hematology, Cambridge Institute for Medical Research and Wellcome Trust and MRC Cambridge Stem Cell Institute, Cambridge University, Hills Road, CB2 0XY Cambridge, UK
[4]Human Genome Sequencing Center, Baylor College of Medicine, Houston, TX 77030, USA
[5]Pasarow Mass Spectrometry Laboratory, Department of Psychiatry and Biobehavioral Sciences and the Semel Institute for Neuroscience and Human Behavior, David Geffen School of Medicine, University of California, Los Angeles, Los Angeles, CA 90095, USA
[6]Huffington Center on Aging, Baylor College of Medicine, Houston, TX 77030, USA
[7]Broad Institute of MIT and Harvard, Cambridge, MA 02142, USA
[8]Department of Stem Cell and Regenerative Biology, Harvard University, Cambridge, MA 02142, USA
[9]Co-first author
[10]Co-senior author
[11]Present address: CeMM Research Center for Molecular Medicine, Lazarettgasse 14, AKH BT 25.3 Vienna, Austria
*Correspondence: wl1@bcm.edu (W.L.), goodell@bcm.edu (M.A.G.)
http://dx.doi.org/10.1016/j.stem.2014.03.002

SUMMARY

To investigate the cell-intrinsic aging mechanisms that erode the function of somatic stem cells during aging, we have conducted a comprehensive integrated genomic analysis of young and aged cells. We profiled the transcriptome, DNA methylome, and histone modifications of young and old murine hematopoietic stem cells (HSCs). Transcriptome analysis indicated reduced TGF-β signaling and perturbation of genes involved in HSC proliferation and differentiation. Aged HSCs exhibited broader H3K4me3 peaks across HSC identity and self-renewal genes and showed increased DNA methylation at transcription factor binding sites associated with differentiation-promoting genes combined with a reduction at genes associated with HSC maintenance. Altogether, these changes reinforce HSC self-renewal and diminish differentiation, paralleling phenotypic HSC aging behavior. Ribosomal biogenesis emerged as a particular target of aging with increased transcription of ribosomal protein and RNA genes and hypomethylation of rRNA genes. This data set will serve as a reference for future epigenomic analysis of stem cell aging.

INTRODUCTION

The function of the hematopoietic system declines with age, manifested by a decreased adaptive immune response and an increased incidence of myeloproliferative diseases, autoimmune, and inflammatory disorders (Linton and Dorshkind, 2004; Ramos-Casals et al., 2003). Although some extrinsic cellular factors such as an inflammatory microenvironment promote aging (Ergen et al., 2012; Villeda et al., 2011), these impact the hematopoietic stem cells (HSCs), causing cell-intrinsic changes that affect the generation of a balanced supply of differentiated blood lineages.

Multiple lines of investigation have established that, with age, phenotypically defined mouse and human HSCs increase in number, whereas lymphoid cell production is diminished, leading to a myeloid-dominant hematopoietic system (Chambers et al., 2007b; de Haan and Van Zant, 1999; Morrison et al., 1996; Rossi et al., 2005). The myeloid dominance is caused partly by a shift in the clonal composition of the HSC compartment (Beerman et al., 2010; Challen et al., 2010; Cho et al., 2008) but also reflects diminished differentiation capacity of individual HSCs (Dykstra et al., 2011).

Mechanisms proposed to account for the age-related loss of HSC function include telomere shortening, accumulation of nuclear and mitochondrial DNA damage (Wang et al., 2012), and coordinated variation in gene expression. Analysis of young and old HSCs revealed that genes associated with inflammation and stress response were upregulated, and genes involved in DNA repair and chromatin silencing were downregulated with HSC aging (Chambers et al., 2007b; Rossi et al., 2005). These earlier studies were conducted on HSC populations that proved to be heterogeneous and therefore represented a mix of cellular phenotypes. Here, we examined highly purified HSCs and tested whether the concept that loss of epigenetic regulation of gene expression in aged HSCs could explain the constellation of aging phenotypes. We completed genome-wide comparisons of the transcriptome (RNA sequencing

[RNA-seq]), histone modification (chromatin immunoprecipitation sequencing [ChIP-seq]), and DNA methylation between young and old purified murine bone marrow HSCs. This report presents an integrated analysis of these genomic properties, reveals potential mechanisms that contribute to HSC aging, and offers a comprehensive reference epigenome of a somatic stem cell type. Finally, it reveals similarities with some common hallmarks of aging (López-Otín et al., 2013) previously noted in model organisms such as *Caenorhabditis elegans* and *Drosophila melanogaster* but not yet examined in mammals.

RESULTS

Alterations in Gene Expression with Age

Because previous analyses of gene expression changes with age utilized HSC populations that are now known to be heterogeneous with regard to lymphoid versus myeloid production proficiency, we utilized the most primitive HSCs with the highest long-term self-renewal potential, which are considered myeloid biased (or lymphoid deficient). HSCs throughout this study were purified as side population (SP)-KLS (c-kit$^+$, lineage$^-$, and Sca1$^+$)-CD150$^+$ (see the Experimental Procedures) because these are found in both young and aged mice and have high phenotypic homogeneity and functional activity (Challen et al., 2010; Mayle et al., 2013). High-throughput sequencing of poly A$^+$ RNA (RNA-seq) from purified 4-month- (4mo) and 24 month-old (24mo) HSCs was performed. With biological duplicates, more than 200 million reads in total for each age of HSC were obtained, offering high sensitivity for detecting gene expression differences in young and aged HSCs.

Comparison of the young and old HSC transcriptomes revealed that 1,337 genes were upregulated and 1,297 were downregulated with HSC aging (false discovery rate [FDR] < 0.05; Table S1 available online). Aging HSC hallmark genes *Clusterin* (*Clu*) and *P-selectin* (*Selp*) (Chambers et al., 2007b) were markedly upregulated, although their expression was also detectable in in young HSCs, demonstrating the sensitivity of RNA-seq.

Gene ontology (GO) analyses indicated that genes upregulated in 24mo HSCs are highly enriched in categories related to cell adhesion, cell proliferation, and the ribosome, whereas downregulated genes are enriched in DNA base excision repair, DNA replication, and cell cycle (Figure 1A). Gene set enrichment analysis with the Molecular Signature Database as well as several customized HSC, myeloid, and lymphoid gene sets (''fingerprint'' genes; Table S2) (Chambers et al., 2007a) revealed that HSC-specific genes as a group were upregulated in old HSCs, in agreement with their increased phenotypic stem cell characteristics. Cell cycle, DNA replication, and glutamate signaling were also differentially expressed gene sets.

The Aging HSC Transcriptome Suggests Reduced TGF-β Signaling

Next, we sought to infer the key regulators responsible for transcriptional changes in aging HSCs. We performed a functional enrichment analysis on the basis of expected cause-effect relationships between transcriptional regulators and their targets in the Ingenuity Pathway Analysis (IPA) database. The most highly represented upstream regulator was growth factor TGF-β1, accounting for ~19% of differential gene expression in young versus old HSCs ($p = 1.96 \times 10^{-33}$; Table S3). In comparison to all genes affected by age, TGF-β-regulated genes were five times more likely to be altered in expression than expected by chance ($p = 3.53 \times 10^{-20}$). As a group, 63% (136 of 217) of TGF-β1 downstream genes were associated with a diversity of biological functions supporting hematopoiesis (n = 83, $p = 4.56 \times 10^{-24}$ to 1.29×10^{-9}) and/or are corroborated by earlier microarray-based studies of HSC aging (n = 86; Table S3).

Depending on the context, TGF-β factors exert pleiotropic, and sometimes opposing, cellular effects. If TGF-β1 signaling were inhibited, then we would expect key intermediary transcription factors (TFs) to be similarly affected. To test this, we constructed a network of cooperating regulators that are connected downstream of TGF-β1 by one edge. This analysis identified Smad3, Sp1, and Egr1 and predicted that they were inhibited during HSC aging (Figure S1 and Table S3). Indeed, expression of *Egr1*, a regulator of HSC homeostasis (Min et al., 2008), is significantly reduced with aging. Additional groups of genes normally activated by TGF-β are of interest. Seven collagen and three metalloproteinase (mmp) genes, implicated in HSC-niche interactions, were downregulated. In addition, expression of TGF-β-regulated genes involved in HSC development, such as *Nr4a1*, *Cepba*, *Jun*, and *Junb*, was reduced. Reduction of several of these targets could contribute to myeloid differentiation bias.

Of genes upregulated with aging, one notable class was ribosomal protein genes, including a majority of those encoding both the large (*Rpl*) and small (*Rps*) subunits (Figure 1B), but not mitochondrial ribosomal protein groups (Mrpl and Mrps; confirmed by exon arrays; Figure S2A). Upregulation of genes involved in protein synthesis has been previously noted with aging. Indeed, inhibition of ribosomal proteins or their regulators has been shown to extend lifespan in yeast and worms (Kaeberlein et al., 2005; Syntichaki et al., 2007). However, changes in the expression of ribosomal protein genes have not been previously reported in mammalian stem cells.

Expression of Key Epigenetic Regulators Decreases with Age

Because we hypothesized that epigenetic regulation plays a role in HSC aging, we examined expression of epigenetic modifiers (Figure 1C). *Ezh1* showed increased expression, consistent with previous findings (Hidalgo et al., 2012). In contrast, *Ezh2* and the polycomb group (PcG) complex member *Cbx2* decreased in old HSCs. In addition, expression of histone kinase genes *Aurka* and *Aurkb*, putative *Ezh2* partners, or targets (Kamminga et al., 2006) also decreased with age.

Genes encoding DNA methyltransferases as a group decreased during aging (FDR = 0.02; Figure 1C and Table S2). Concomitantly, genes encoding Tet1 and Tet3 DNA demethylation proteins were also decreased. Although their functions are unknown, *Tet2* mutation leads to expansion of hematopoietic progenitors and increased stem cell self-renewal (Ko et al., 2011; Li et al., 2011; Moran-Crusio et al., 2011; Quivoron et al., 2011), and TET2 is recurrently mutated in myelodysplastic syndrome (MDS) and acute myeloid lymphoma (AML) patients (Delhommeau et al., 2009; Langemeijer et al., 2009). Consistent

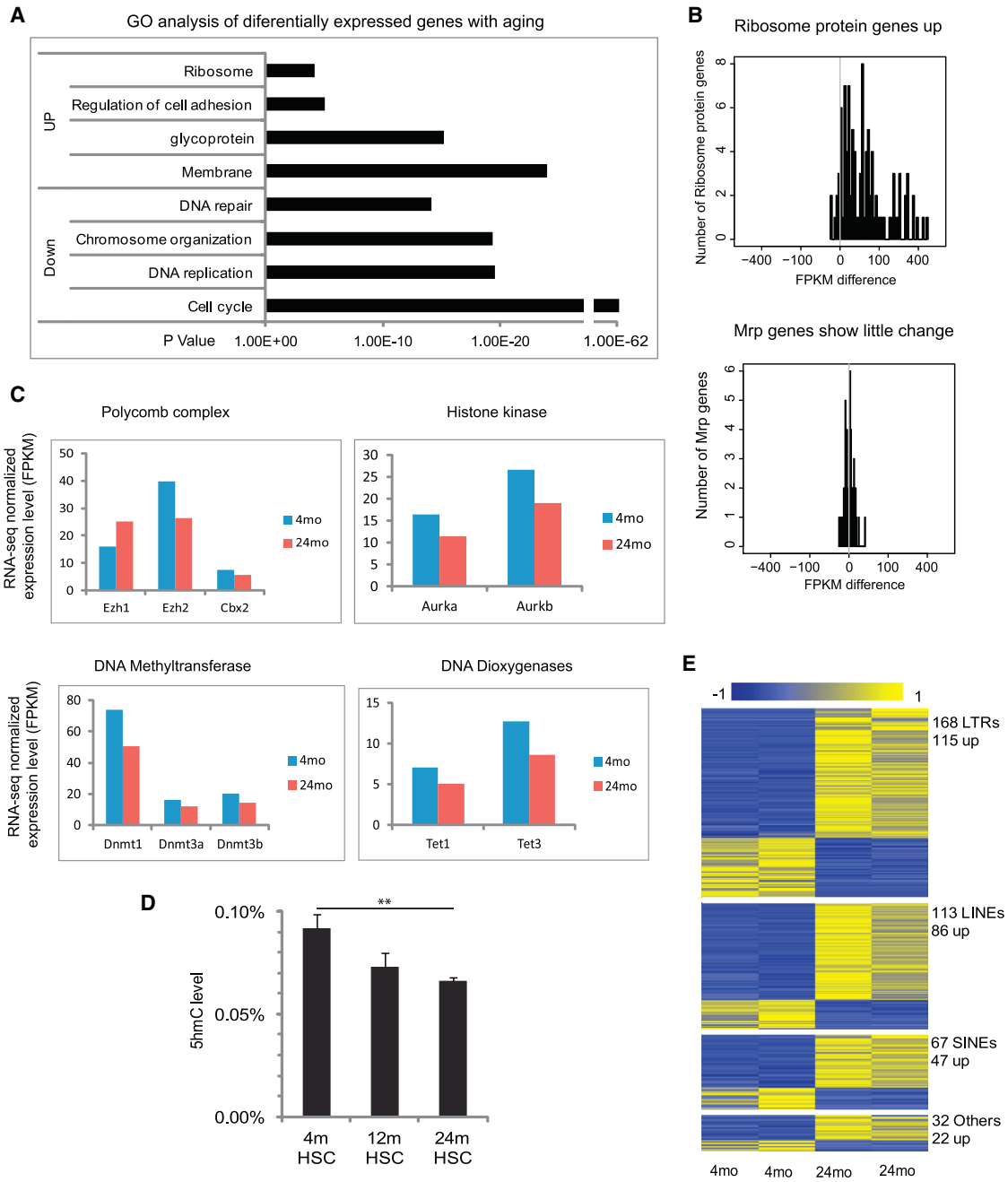

Figure 1. Transcriptome Alterations with HSC Aging

(A) Gene ontology (GO) enrichment analysis for differentially expressed genes with HSC aging. The x axis shows the p value.

(B) The distribution of expression changes for ribosomal protein genes during HSC aging where the x axis value is fragments per kilobase of exon per million fragments mapped (FPKM) difference between old and young HSCs.

(C) Average FPKM value of genes encoding epigenetic modifiers in young and old HSCs.

(D) HPLC mass spectrometry measurements of 5-hydroxy methylcytosine (5hmc) levels as a proportion of the total cytosine in purified HSCs from 4mo, 12mo, and 24mo mice (n = 7). Error bars represent mean ± SEM. **$p < 0.01$ and ***$p < 0.005$ (Student's t test).

(E) Differential expression of repetitive elements during HSC aging. Each row represents a repeat location in the genome. Blue denotes low expression, and yellow high expression (log2 reads number).

See also Figures S1 and S2.

with reduction of Tet gene expression, quantitative mass spectrometry revealed reduced 5-hydroxymethycytosine with age (Figure 1D).

Repetitive elements are epigenetically repressed, so we examined whether they were dysregulated with aging. Strikingly, the RNA-seq data revealed marked changes in the expression of

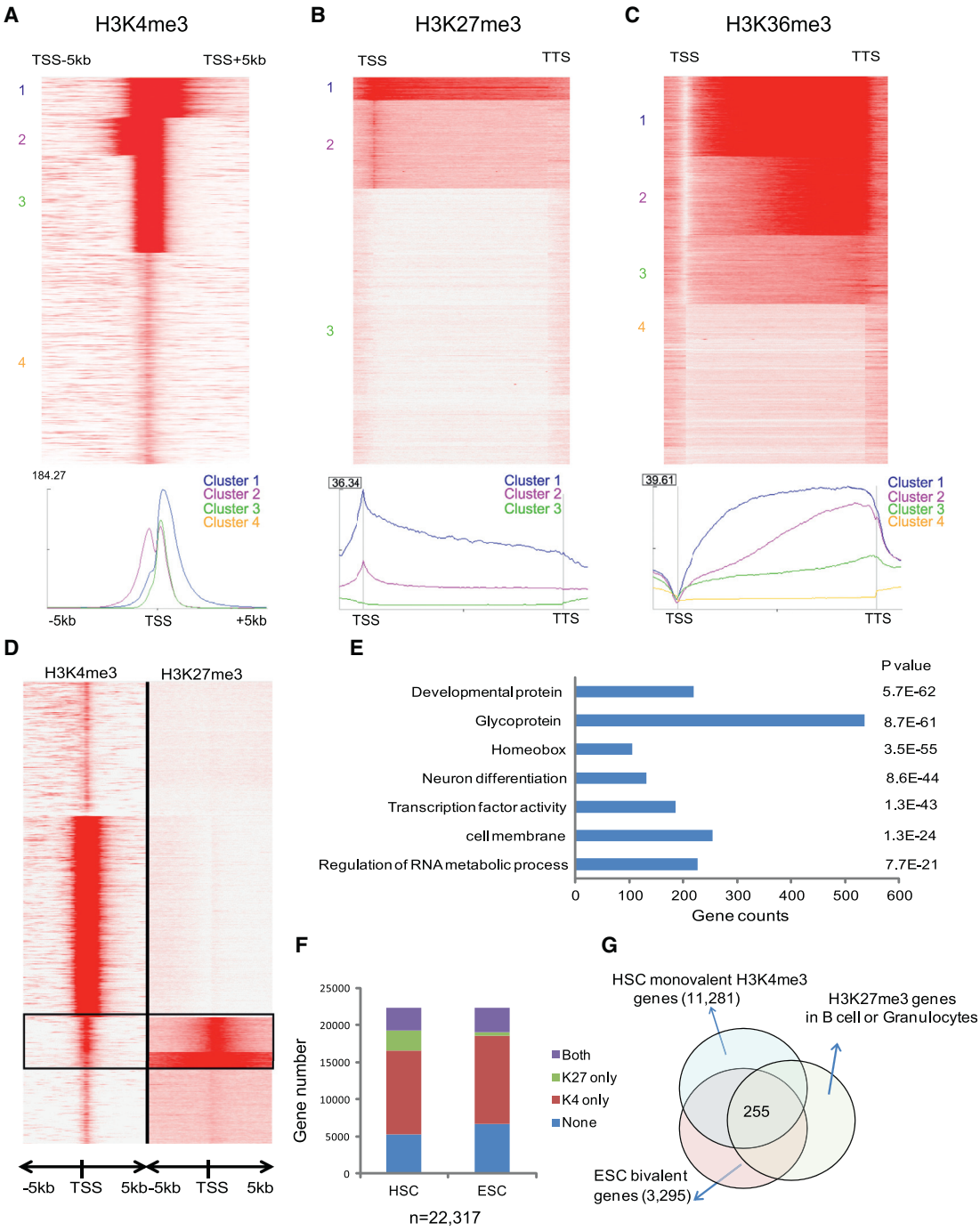

Figure 2. Histone Marks in HSC

(A) Heat map and profile of H3K4me3 around TSS of all RefSeq genes. Red represents high intensity, and white represents no signal. Cluster IDs are marked to the left. The profile plot shows the average reads per region on the y axis at each relative position to TSS on the x axis for the four clusters with H3K4me3 coverage.

(B) Heat map and profile of H3K27me3 around the gene body of all RefSeq genes. The profile plot shows the average reads per region on y axis at each relative position on the x axis for the three clusters with H3K27me3 coverage. All genes are normalized to same length.

(C) Heat map and profile of H3K36me3 around the gene body of all RefSeq genes. The profile plot shows the average reads per region on the y axis at each relative position on the x axis for the four clusters with H3K36me3 coverage. All genes are normalized to same length.

(D) Unsupervised clustering of histone profiles around the TSS of the RefSeq genes showed bivalent genes marked by both H3K4me3 and H3K27me3 in HSCs.

(E) GO enrichment analysis for the bivalent genes in HSCs. p values and gene counts are shown.

(legend continued on next page)

multiple repetitive elements with age, including 168 long terminal repeat (LTR) elements, 113 long interspersed elements (LINEs), 67 short interspersed elements (SINEs), and 32 other repeat elements. Of these, 68%∼76% exhibited increased expression. This increased repetitive element expression may result from aberrant epigenetic repression and could contribute to increased genome instability (Figure 1E). Anomalous repetitive element expression has been associated with embryonic stem cells (ESCs) (Xie et al., 2013) but not aging. Examination of the genes near the dysregulated LTR elements, LINEs, and SINEs revealed 194, 127, and 72 genes, respectively. Functional enrichment with the Genomic Regions Enrichment of Annotations Tool indicated LINE- and SINE-associated genes were enriched for these involved in hematological diseases such as *Cdc42*, *Flt3*, and *Lmo2* (Table S4).

Alterations in Transcript Isoform Expression

RNA-seq also revealed age-associated changes in promoter usage and pre-mRNA abundance. We identified 118 genes that showed switched promoter usage during aging (Table S4). One example is *Runx1t1*, a locus translocated to *RUNX1* in some types of AML. The full-length *Runx1t1* is expressed in old HSCs, and the short isoform is expressed in young HSCs (Figure S2B). Another example is *Nfkbiz*, with expression of the short isoform decreased with aging (Figure S2C).

We previously noted that HSCs contain significant incompletely spliced mRNA that is reduced when HSCs are activated (Venezia et al., 2004). Global pre-mRNA quantification confirmed a full 13% of reads within RefSeq introns in young HSCs, which decreased with age (Figure S2D). Nearly 300 genes showed age-associated alteration of pre-mRNA abundance. Of the 184 genes with decreased pre-mRNA abundance, many were classified in ribosome, immunoglobulin domain, and extracellular region categories by GO analysis (for example, *Ctla2a* and ribosome protein *Rpl13*; Figure S2E), whereas the 96 genes with increased pre-mRNA were enriched in zinc-finger-encoding genes (Figure S2F). The decreased pre-mRNA with age may be associated with increased translation.

HSC-Specific Chromatin Features

To examine epigenetic alterations, we profiled the principal regulatory chromatin marks in HSCs, specifically H3K4me3, H3K27me3 and H3K36me3 marks in young (4mo) and old (24mo) HSCs with the use of ChIP-seq. Because these global analyses have never been performed on such highly purified HSCs, we first describe our general observations.

In young HSCs, 10,263 RefSeq genes had clear H3K4me3-associated peaks. Clustering of the signal around the transcription start site (TSS) show that the H3K4me3 peaks can be classified into four distinct clusters (Figure 2A). Cluster 1 overlaps with 2,373 genes and shows high intensity and wide coverage (mean 3,200 bp) into the gene body. Cluster 2 (2,225 genes) and cluster 3 (5,665 genes) have similar intensity and coverage lengths (∼2,000 bp), but cluster 2 has more coverage upstream of the TSS. The remaining RefSeq genes have little or no discernible H3K4me3 peak (cluster 4).

For the repressive H3K27me3 mark in young HSCs, we identified 3,768 peaks present in the promoter region defined as the TSS ± 1 kb. Unsupervised clustering showed the majority with a sharp peak over the TSS (cluster 2; distinct from the H3K4 clusters). A small subset showed high levels spread over most of the coding region (cluster 1; Figure 2B). For H3K36me3, the signals are depleted at the TSS and increase from the TSS to the transcription termination site (Figure 2C). As in other cell types, this mark was strongly correlated with gene expression and enriched in the gene body. H3K36me3 and H3K27me3 signals were generally mutually exclusive (Figure S3A).

Genes with both activating H3K4me3 and repressive H3K27me3 were first identified in ESCs as so-called "bivalent" genes, thought to represent poised master regulators (Bernstein et al., 2006). Here, 2,267 out of 3,768 H3K27me3-enriched genes in HSC also contain H3K4me3 (Figure 2D), similar to the proportions in ESCs (although we cannot confirm that the marks are on the same allele). These genes were enriched for development, transcriptional regulation, and RNA metabolism GO categories (Figure 2E), consistent with previous observations (Weishaupt et al., 2010). Many transcription factors important for hematopoietic differentiation, such as *Cebpa*, *Ebf-1*, *Pax5*, and *Gata3*, appeared bivalent. Notably, one-third of the bivalent HSC genes are glycoproteins involved in signaling pathways such as Wnt, Hedgehog, bone morphogenetic proteins, and TGF-β. Their expression was generally low (Figure S3B).

Next, we attempted to identify potential HSC regulators on the basis of histone modifications. We compared ESC H3K4me3 and H3K27me3 binding sites (Bernstein et al., 2006) with those from HSCs as well as differentiated B cells and granulocytes (Gr) (Figure 2F). We selected genes that were developmental regulators (bivalent in ESCs) and were activated in HSCs (H3K4me3 only) but were repressed upon HSC differentiation (regained H3K27me3 in differentiated B cells and Gr) to identify 255 genes (Figure 2G and Table S5). These are enriched for TFs and pathways in cancer (Figure S3C). Significantly, 20% of them overlap with HSC fingerprint genes (Chambers et al., 2007a), including *Cd34*, *Gata2*, and *Meis1*, whose functions in HSCs have been demonstrated, showing that histone profiles can independently predict key HSC regulators.

Aging-Associated Changes in Histone Marks

Next, we examined aging-associated histone mark changes. Although most shifts were moderate, there were some unique features. Old HSCs exhibited a 6.3% increase in the number of H3K4me3 peaks, many of which were considerably broader with age; more than half of all H3K4me3 peaks expanded, and less than 10% shrank (Figure 3A). The expansion of H3K4me3 coverage was greatest for peaks already broad in young HSCs; for peaks longer than 3 kb in young HSCs, there are 69% and 7% of lengthening and shortening events, respectively

(F) The classification of RefSeq genes according to cobinding patterns of H3K4me3 and H3K27me3 in HSCs and ESCs. Both, H3K4me3 with H3K27me3.
(G) Venn diagram showing the HSC genes that share the listed chromatin modifications: bivalent in ESCs, actively transcribed in HSCs, and repressed (H3K27me3) in differentiated B and Gr1 cells.
See also Figure S3.

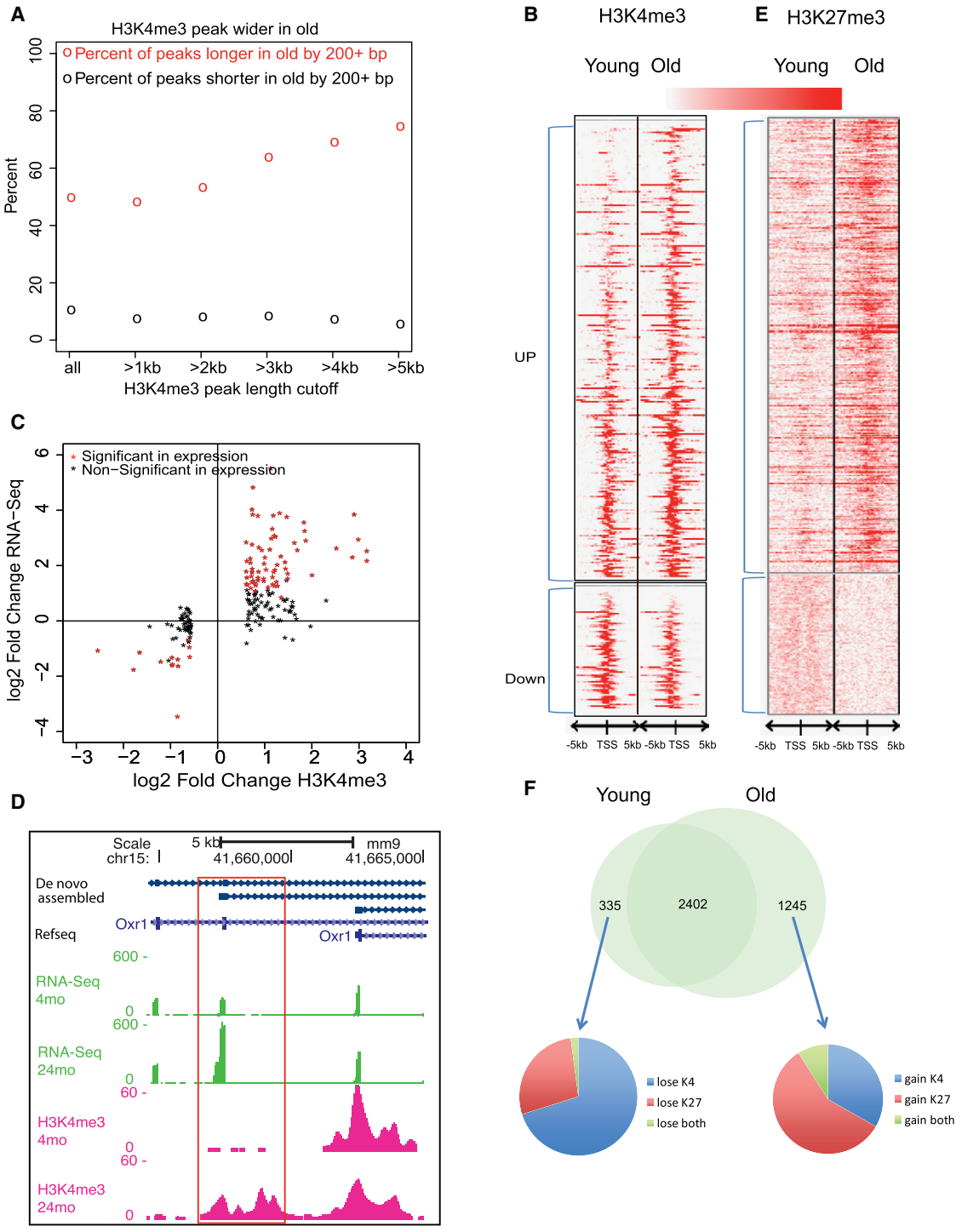

Figure 3. Histone Modifications Changes with HSC Aging

(A) Percent of H3K4me3 peaks getting longer or shorter (>200 bp) in old HSCs. The x axis is the peak length cutoff to be counted toward lengthening or shortening. The y axis is the number of wider or shorter peaks divided by total number of peaks at the length cutoff. The circles represent the percent of lengthening (red) and shortening (black) events.

(B) Heat map of H3K4me3 density around promoters that show significantly different H3K4me3 binding with age (Poisson $p = 10^{-8}$).

(C) The correlation between gene expression and H3K4me3 signals for the significantly different H3K4me3 binding genes. The x axis denotes the log2 fold change of H3K4me3 ChIP-seq read counts in the defined promoter region, and the y axis denotes the log2 fold change of FPKM value for the gene.

(legend continued on next page)

(Figure S3D). Peak expansion was particularly striking at genes associated with HSC identity (Figure S3E).

More H3K4me3 coverage in old HSCs suggested that some previously unexpressed transcripts are activated. The levels of H3K4me3 were significantly increased on 267 promoters and decreased on 73 promoters in the old HSCs (Figure 3B). We observed a strong positive correlation between altered H3K4me3 signal and gene expression changes (Figure 3C). Increased H3K4me3 was observed for the most upregulated genes, such as *Selp*, *Nupr1*, *Sdpr*, *Plscr2*, and *Slamf1*, and genes in the *HoxB* cluster (Figure S3F). In addition, increased H3K4me3 was associated with altered promoter usage, for example, at the *oxidation resistance 1* (*Oxr1*) gene, revealing an unannotated promoter (Figure 3D).

PcG-mediated epigenetic alteration is considered a driving force behind many age-related changes and is often dysregulated in human malignancies. We observed similar H3K27me3 peak counts with age but increased length of coverage by 29% from 203 to 261 Mb, and the average signal intensity at the TSS increased by ~50%, similar to quiescent satellite cells (Liu et al., 2013). H3K27me3 binding increased at 402 promoters and decreased at 124 promoters (Figure 3E). Notably, at the *Flt3* locus, H3K27me3 was increased and expression decreased (Figure S3G), consistent with the diminished lymphoid differentiation potential of aged HSCs.

One well-known target of the PcG family during aging is *Cdkn2a* (encoding $p16^{INK4a}$), which showed progressive loss of H3K27me3-associated repression and increased expression with aging in neural stem cells (Molofsky et al., 2006). Increased Cdkn2a is considered a primary indicator of cellular senescence in virtually all tissues in mice and humans (López-Otín et al., 2013). However, HSCs represent a stark exception; our results show that $p16^{INK4a}$ is a bivalent gene effectively repressed by H3K27me3 in both 4mo and 24mo HSCs, and its expression remains undetectable at either age (Figure S3H). These data argue against the notion that loss of function of HSCs with age is due to the acquisition of a senescent state linked to p16.

Considering the global changes of H3K4me3 and H3K27me3 with HSC aging, we reexamined the bivalent domains. The results indicated that 335 bivalent domains disappear in old HSCs, whereas 1,245 emerge, largely because a gain of both H3K4me3 and H3K27me3 or H3K27me3 only (Figure 3F). The genes that lose H3K27me3 are enriched for the category of membrane protein, whereas the genes that gain H3K27me3 are enriched for glycoprotein and cell adhesion (Figure S3I and Table S5).

HSC-Specific Methylome

We also examined DNA methylation changes with aging. Global CpG hypomethylation associated with aging has been observed in many tissues and is thought to contribute to genome instability and the risk of neoplastic transformation (Maegawa et al., 2010). Here, we used whole-genome bisulfite sequencing (WGBS) and generated 1,494 million (4mo HSCs) and 1,493 million (24mo HSCs) reads; about 82.6% and 84.3%, respectively, were aligned to the reference genome (mm9). Of all cytosines present in the reference genome, about 93% of Cs and 99% of CGs were covered in both data sets, with an average coverage of 46-fold (4mo) and 50-fold (24mo).

Globally, the HSC methylome exhibited the DNA methylation patterns in line with those observed in other mammalian cells (Stadler et al., 2011). Low DNA methylation was found in CpG islands (CGIs) and promoters, and high methylation was found in gene bodies and repetitive elements (Figures 4A and S4A–S4C). Bivalent domains showed the lowest DNA methylation (5%; Figure S4D), which was consistent with the inverse correlation of DNA methylation and H3K4me3 (Meissner et al., 2008). In contrast, H3K36me3-enriched regions are associated with the highest DNA methylation (94%), possibly because of Dnmt3a and H3K36me3 interaction (Dhayalan et al., 2010). Interestingly, the CGI methylation is diverse and dependent on the genomic or epigenomic context (Figure S4E).

We also compared the HSC and ESC (Stadler et al., 2011) methylomes. 5% of CGIs show differential methylation between these two stem cell types, with 689 CGIs hypermethylated and 130 CGIs hypomethylated in HSCs (Figure 4B). Furthermore, we identified differentially methylated regions (DMRs) between HSCs and ESCs as a region of at least 100 bp in length wherein consecutive CpGs show the same hyper- or hypomethylation state. Analysis showed striking enrichment of positive TF regulation for hypo-DMR genes and negative TF regulation for hyper-DMR genes. Of ten well-known hematopoietic TFs (Wilson et al., 2010), all had hypomethylated promoter regions, and their target binding sites were also hypomethylated. For example, the *Runx1* promoter is methylated in ESCs and unmethylated in HSCs (Figure 4C), and its binding sites showed a strong bias toward hypomethylation in HSCs (Figure 4D). Altogether, the general methylation pattern in different genomic regions is conserved in HSCs, but the methylation of cell-type-specific TFs and their binding sites is unique to HSCs.

Aging-Dependent DNA Methylation and Interaction with Histone Modifications

In contrast to the age-associated hypomethylation observed in somatic cells, HSCs showed methylation increasing with age from 83.5% to 84.6% in old HSCs, which was consistent with previous studies focused on CGIs (Beerman et al., 2013). We observed a total of 448,166 differentially methylated CpGs (DMCs; ≥20% difference), of which 38.5% were hypomethylated (hypo-DMCs) and 61.5% were hypermethylated (hyper-DMCs). For different genomic features (Table S6), a slightly greater DNA methylation increase was observed for the gene body, LINEs, and SINEs, whereas CGIs and promoters showed balanced increases and decreases (Figure 5A). DNA encoding for rDNA was a hotspot for hypo-DMCs (Figure 5B). CpGs with an intermediate methylation ratio were more susceptible to alterations than fully methylated or unmethylated CpGs (Figure S5A). We also found that increased H3K4me3 strongly

(D) Genome browser view on the *Oxr1* gene body. The boxed area shows an unannotated promoter with H3K4me3.
(E) Heat map of H3K27me3 density around promoters that show significantly different H3K27me binding with age.
(F) Venn diagram showed bivalent domains change with HSC aging.
See also Figure S3.

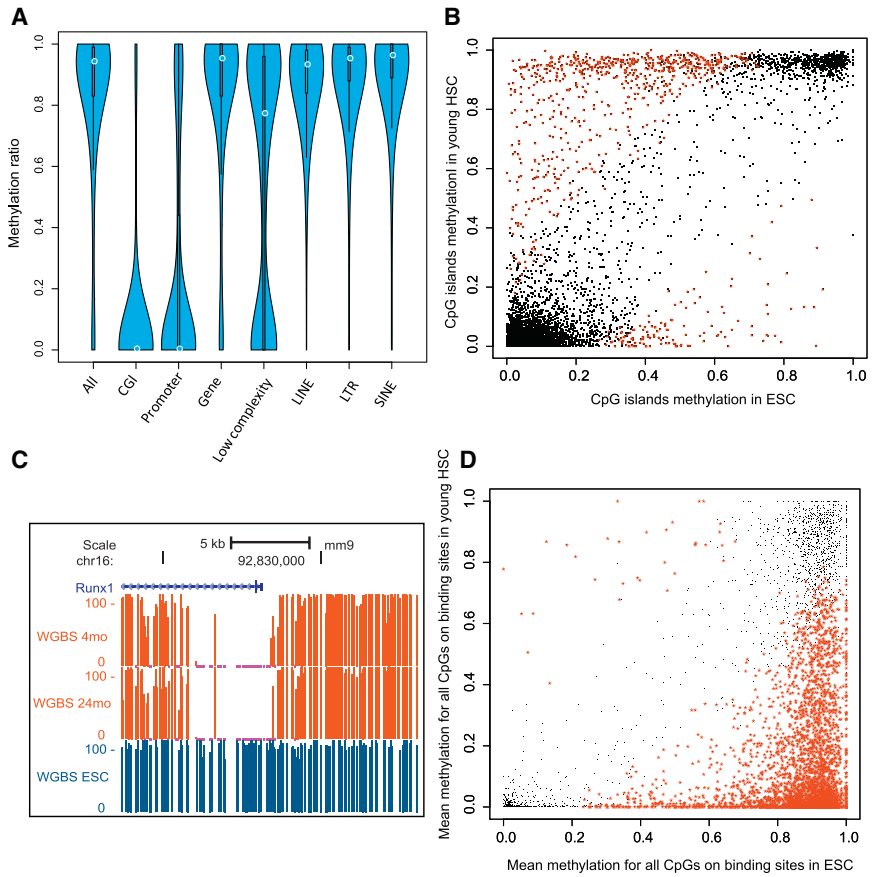

Figure 4. HSC-Specific Methylome

(A) Violin plot showing DNA methylation ratios in different genomic features. The thickness of the bars indicates densities of CpGs at the y axis ratio, and the white circle indicates the median.

(B) Scatter plot for mean methylation ratio for all the CpGs of each CGI in HSCs in comparison ESCs. The x and y axes indicate the methylation ratio of each CGI in HSC and ESC respectively. The black dots represent loci that are not significantly different between the cell types, and the red stars represent the CpG Islands that exhibit cell-type-specific methylation.

(C) Genome browser view showing the percentage of methylation in the promoter of the *Runx1* gene in young and old HSCs and ESCs.

(D) Methylation ratios in HSCs versus ESCs of Runx1 binding sites as mapped in mouse HPC7 hematopoietic progenitor cells. Black and red are as denoted in (B).

See also Figure S4.

correlated with hypomethylation, H3K27me3 regions are hot spots for both hypo- and hyper-DMCs (Table S6), and decreased H3K36me3 correlated with hypo-DMCs (Figure 5C).

To identify the genes or pathways subject to DNA methylation alterations, we screened the methylome for DMRs. We identified 4,828 hypo- and 4,523 hyper-DMRs between 4mo and 24mo HSCs that were associated with 2,253 and 2,071 genes, respectively (Table S7). Calculating the Pearson correlation between the methylation and gene expression changes, we discovered that DMRs between the TSS and the 1 kb immediately downstream showed the highest correlation with gene expression (−0.312) followed by the DMRs in the promoters lacking CGIs (−0.250; Figure S5B). Hypo-DMR-associated genes are enriched for pathways in cancer and include *Bcl2*, *Ptk2*, *Rb1*, *Mll3*, *Runx1*, *Flt3l*, *Myc*, *Igf1*, *Igf1r*, *NFkb2*, *Tgfb3*, and *Tgfbr2*. In contrast, both hypo- and hyper-DMR genes are enriched in old HSCs for cell adhesion and actin cytoskeleton, such as *Arpc1a*, *Ablim2*, *Cadm1*, *Cdh1*, *Col2a1*, *CD34*, *CD40*, and *CD86* (Figure S5C and Table S7).

DNA hypermethylation on polycomb-targeted genes is a hallmark of cancer and aging. Here, we compared H3K27me3-marked genes in both young and old HSCs with the DMR gene list. We found that 40% of hyper-DMR genes contain H3K27me3 marks, whereas 25% of hypo-DMR genes contained H3K27me3, confirming that polycomb-targeted genes are hotspots for aging-related DNA methylation (Figure 5D). One example is *Nr4a2*, a regulator of HSC quiescence (Sirin et al., 2010), which gained methylation on the H3K27me3-marked domain with age and correlated with suppression of the short isoform (Figure S5D). To examine whether an epigenetic signature alone might identify potential biomarkers of aging, we identified ~50 genes that showed concomitant DNA methylation and histone H3K4me3 differences during HSC aging (Figure 5E). These loci showed a particularly strong inverse correlation between their age-related decrease in DNA methylation and their increased H3K4me3 (64%; Figure S5E), but not all of them showed increased gene expression (Figure S5F). These results indicate that the epigenetic state may be used to predict aging independent of gene expression.

Aging-Associated DNA Methylation Interferes with the Transcriptional Network

Previous DNA methylation studies showed that hypomethylated regions are usually associated with cell-specific regulatory regions or TF binding sites (Hodges et al., 2011; Stadler et al., 2011; Ziller et al., 2013). To determine whether the methylation states in such regulatory regions change with HSC aging, we examined the methylation ratio in the binding sites of five TFs associated with HSC pluripotency, including Scl, Erg, Gata2, Runx1, and Ldb1 (Wilson et al., 2010). Although basal methylation levels for these TF binding sites in HSCs are low (Figure S6A), methylation at Gata2 and Ldb1 binding sites are further reduced with age (Figure S6B). This led us to further test whether aberrant DNA methylation disrupts the HSC transcriptional networks more broadly. We compiled genome-wide binding sites of more than 150 TFs found in a variety of blood lineages (>10) and compared them with DMRs identified in young and old HSCs. The results revealed that hypo-DMRs are significantly enriched for Ring1b, Scl, Gata1, Ldb1, and Runx1 binding sites in old HSCs but not for Rad21 binding sites, which served as a

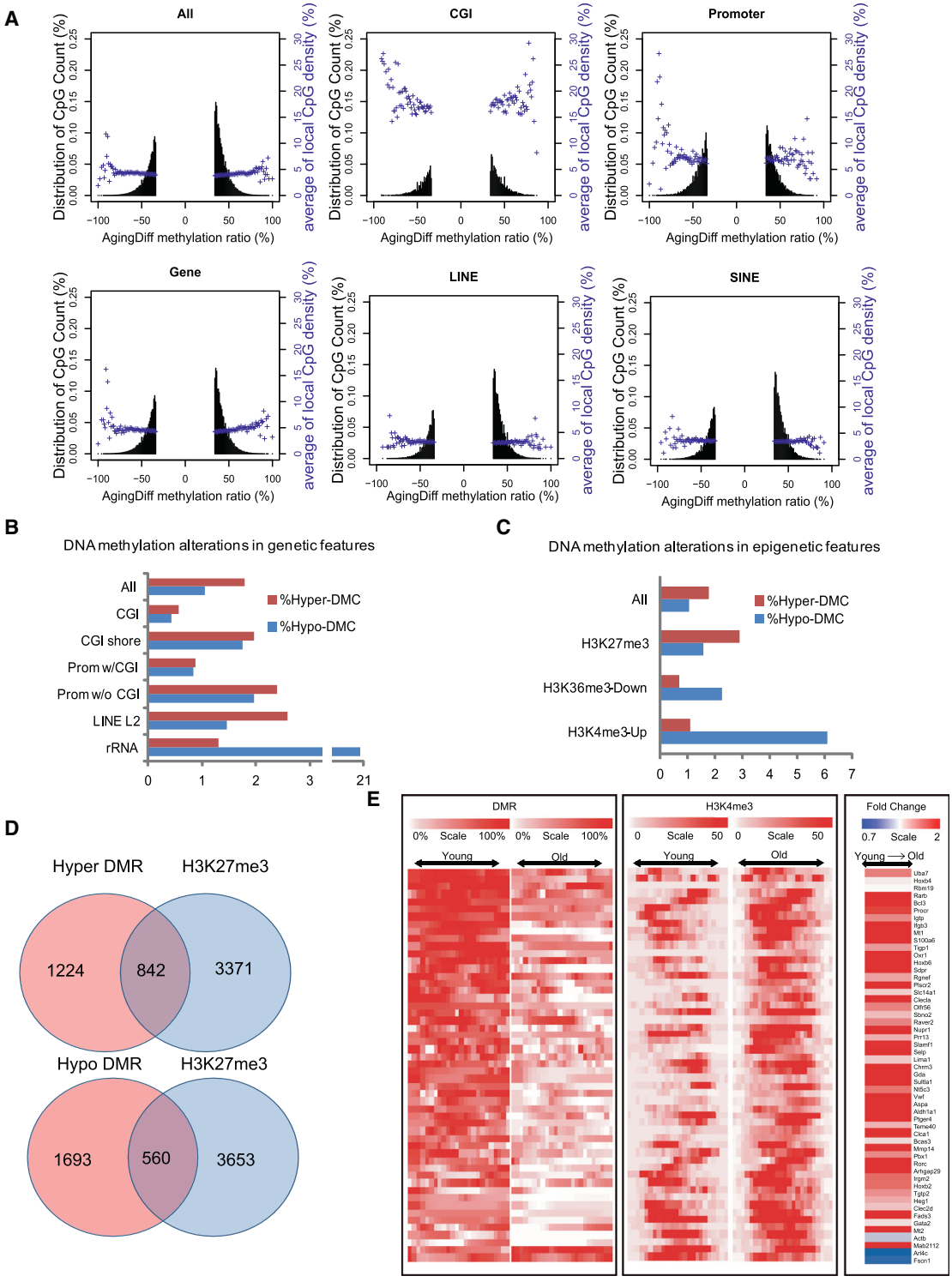

Figure 5. HSC Methylome Alterations with Aging

(A) Plots show the degree of differential methylation in young versus old HSCs and the relationship between the local CpG density (blue). The top left plot shows all DMCs in old HSCs defined as CpGs that are ≤20% less methylated and ≥20% more methylated. The other plots show DMCs located within different genomic features.

(B) The percentage of hyper- (red) or hypo- (blue) DMCs in different genomic features.

(C) Interaction of DNA methylation and histone modifications. The percentage of DMCs in the indicated epigenetic features and their alterations with aging are also shown.

(legend continued on next page)

negative control (Figure 6A). Combinatorial interactions of Scl, Lyl1, Gata2, Runx1, Lmo2, Fli1, and Erg have been suggested to form a central transcription network that regulates HSC pluripotency (Wilson et al., 2010). Therefore, hypomethylation of the binding sites for some of these factors or related family members may play a role in reinforcing the self-renewal program in HSCs. In parallel, hyper-DMRs are highly enriched for Pu.1, Fli1, Gfi1, and Erg binding sites in old HSCs (Figure 6B). Among them, binding sites of Pu.1, which promotes HSC differentiation, showed hypermethylation with the highest statistical significance (Figure 6C). Given that mutation or deletion of *PU.1* is leukemogenic (Cook et al., 2004), hypermethylation of its binding sites may increase the risk for myeloid leukemia.

We also examined changes with age in methylation of canyons, which comprise around 1,100 large regions with low methylation enriched for genes involved in transcriptional regulation (Jeong et al., 2014). Hypomethylation is 25% to 28% more frequent at inner edges of canyons, whereas hypermethylation is 25% more frequent at outside edges (Figure 6D). Furthermore, canyons with more hypomethylated DMCs are associated with greater H3K4me3 coverage, whereas canyons with more hypermethylated DMCs show a distinct shift in H3K27me3 occupancy characterized by both a substantial decline in partial coverage (spanning < 25% of canyon length) and an increase in broader H3K27me3 coverage (spanning > 90% of canyon length; Figure 6E). This is similar to the behavior of canyons after *Dnmt3a* KO (Jeong et al., 2014).

All of these findings suggest that DNA methylation is a critical layer of epigenetic regulation controlling HSC aging and underscore some of the similarities between the epigenetic changes with aging and those in *Dnmt3a* knockout HSCs.

Methylation Alterations Identify HSC Regulators and Age-Associated Phenotypes

To determine whether changes in DNA methylation were likely to affect HSC function, we compared DMR genes with HSC myeloid and lymphoid fingerprint genes. Strikingly, of HSC fingerprint genes, 70% showed hypomethylation (Table S7), which correlated with their increased expression (−0.45; Figures 7A and S7A). Hypermethylation and decreased expression was also observed on a subset of HSC fingerprint genes. To test whether their decreased expression might explain HSC aging phenotypes, we selected the imprinted gene *Slc22a3* encoding a solute carrier family member (Gründemann et al., 1998), for further characterization (Figure 7B). To examine its function, we transduced progenitors from young mice with a retroviral microRNA (miRNA) knockdown construct. After 2 days of culture, transduced cells were sorted for quantitative RT-PCR (qRT-PCR) in order to confirm a knockdown efficiency of about 60% (Figure 7C), mimicking its expression change in old HSCs. Although transplantation showed knockdown of *Slc22a3* did not affect engraftment, there were a greater proportion of myeloid cells generated from *Slc22a3* knockdown HSCs (Figure 7D). Thus, decreased expression of *Slc22a3* may contribute to the myeloid-biased differentiation of old HSCs.

MDS is a hematologic disorder that increases dramatically with age. We considered whether some of the changes associated with normal HSC aging were associated with MDS. We examined 66 MDS-related genes as defined by IPA. Of these, 21 contained a DMR ($p = 1 \times 10^{-16}$), and their methylation changes were generally inversely correlated with gene-expression changes (Figure 7E). Five contained both hypo- and hyper-DMRs, such as *Hspa1a* (Figure S7B). Notably, the gene for splicing factor *Sf3b1* contains a hyper-DMR at its TSS region and shows decreased expression. Somatic mutation of this gene has been found in 20% of MDS patients (Papaemmanuil et al., 2011). The disordered methylation on those MDS-associated genes may contribute to the development of this disease.

DISCUSSION

In summary, we present a comprehensive report of the transcriptome and epigenetic signatures, including DNA methylation and three histone modifications, of highly purified young and old HSCs, which can serve as a resource for both normal and aging adult stem cell studies. The epigenetic alterations are closely correlated with the phenotypic and functional changes that have been documented for HSCs, namely the increased HSC self-renewal, diminished differentiation potential, and biased ratio of myeloid versus lymphoid differentiation. Although not directly pathological, the epigenetic changes we observe clearly provide a cellular environment conducive to age-related pathologies, such as MDS and leukemia, as outlined below.

Age-Related Changes Suggest Reduced TGF-β Signaling

Our analyses of the transcriptome of young and old HSCs strikingly implicate TGF-β as likely to be among the most significant contributors to the functional age-related declines that occur in this stem cell type with age. Although decreased TGF-β signaling has been implicated in aging of cardiac and neural tissue (Blaney Davidson et al., 2005; Loffredo et al., 2013), we observed genes involved in specific signaling modules that are most likely mediating the altered TGF-β response. In the context of HSCs, we are inferring responses to stimuli that are most likely initiated by the niche based on the large number of dysregulated TGF-β genes.

For each step of the TGF-β1 signaling pathway, there are a number of differentially expressed genes in aging HSCs. For example, genes involved in ligand activation or bioavailability were decreased, such as matrix metalloproteases *mmp-2* and *mmp-9* (Yu and Stamenkovic, 2000). We also observed decreased expression of the gene for Smad6, which interferes with phosphorylation of Smad2 (Imamura et al., 1997) and Smad cofactors p300, Crebbp, and Atf3. Given these data, as

(D) Venn diagram showing the overlap of DMR genes with polycomb repressed genes in HSCs.
(E) Heat map of DNA methylation, H3K4me3 signal, and expression values for 50 potential HSC aging markers. Each row represents a gene-associated region where there is coexistence of differential H3K4me3 and DNA methylation. For H3K4me3 and DNA methylation, red denotes high methylation and white denotes no methylation. For gene expression, red denotes upregulation and white denotes downregulation.
See also Figure S5.

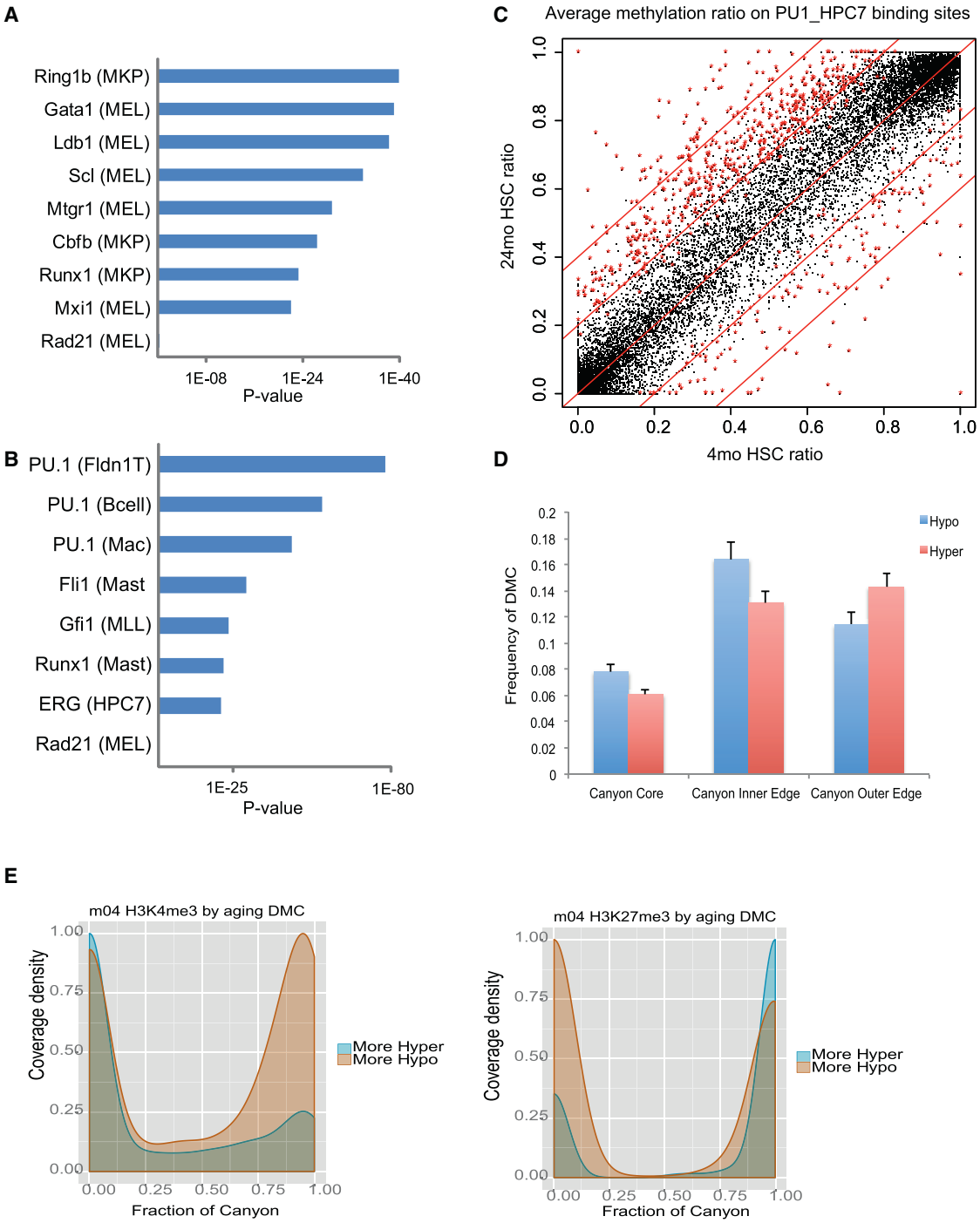

Figure 6. DNA Methylation Changes Interact with Transcriptional Network

(A) Hypo-DMRs are enriched for the indicated TF binding sites. Parentheses identify the cell type or cell line in which the TF binding sites were originally identified. MKP, megakaryocyte progenitors; MEL, murine erythroleukemia cell line.

(B) Hyper-DMRs are enriched for TF binding sites in distinct blood lineages. Parentheses identify the cell type or cell line in which the TF binding sites were originally identified. FLDN1_T, fetal liver DN1 T cell; Mac, macrophage; Mast, mast cells; MLL, MLL/ENL-expressing preleukemia cells; MEL, murine erythroleukemia cell line.

(C) Scatter plot comparing the methylation ratio for all the Pu.1 binding sites identified in the HPC7 cell line between 4mo and 24mo HSCs. Red symbols indicate binding sites with methylation ratios significantly changed between 4mo and 24mo HSCs.

(D) Average number of CpGs in DNA methylation canyon regions differentially methylated between 4mo and 24mo HSCs. Canyons are defined in 12mo HSCs. DMCs counts are normalized by region length. Canyon core, region inset by 500 bp on each edge; inner and outer edge, 500 bp regions inside and outside canyon edges, respectively. Error bars represent mean ± SEM. **p < 0.01 and ***p < 0.005 (Student's t test).(E) H3K27me3 (left) and H3K4me3 (right) peak coverage

(legend continued on next page)

well as the long-standing evidence for a role in TGF-β signaling on HSC function (Fan et al., 2002; Jacobsen et al., 1995), further study of the role of TGF-β signaling in HSC aging is warranted.

Significance of the Altered Ribosomal Gene Transcription

In the transcriptome, epigenome, and methylome data, we found that genes included in the GO category ribosome were a prominent target of aging. In particular, the decreased ribosomal protein gene pre-mRNA levels suggest more efficient splicing and possibly translation. Even though aged HSCs are not more in cycle than young HSCs (Chambers et al., 2007b; Rossi et al., 2005), they may be more activated. Intriguingly, defects in ribosome biogenesis have been linked to bone marrow failure syndromes associated with a risk of developing malignancies, such as Diamond-Blackfan anemia (Narla and Ebert, 2010). In addition, ribosomal biogenesis has repeatedly been linked to aging in model organisms (Curran and Ruvkun, 2007; Grewal, 2009; Hamilton et al., 2005; Pan et al., 2007) but not yet in mammals. Our data suggest that a reexamination of the role of the ribosome in mammalian stem cell aging should be undertaken.

Consistency of HSC Aging with General Organismal Aging

Our observations regarding the increase in H3K4me3 peaks and the increased length of many of the peaks is striking in the context of recent observations in *C. elegans* where mutation of genes involved in H3K4 methylation increased longevity (Greer et al., 2010). This phenomenon was dependent on a histone demethylase (Greer et al., 2011), indicating that sustained H3K4 methylation activity promotes aging. Although we do not identify loss or gain of H3K4 methyltransferases, the accumulation of H3K4me3 with age, particularly on genes in which H3K4 trimethylation is already broad, most likely contributes to the dysfunction of HSCs in the older animals. Notably, the genes associated with increased H3K4me3 breadth are specifically those associated with stem cell self-renewal and loss of differentiation capacity. Thus, the increase of this activating mark on these particular genes may be linked to the functional changes that occur in aged HSCs. We reanalyzed data from a recent study on aging of muscle satellite cells (Liu et al., 2013) and found that H3K4me3 length also increased by about 5% with age (data not shown). It will be important to extend these observations of H3K4me3 to other aging systems and identify the critical targets and mechanisms.

Relationship between Normal HSC Aging and Myeloid Malignancies

MDS and AML are increasingly common with age. Although heterogeneous, both of these diseases are marked by impeded differentiation and a shift toward myeloid output. Our data suggest that, even in the absence of discernable mutations, aging HSCs acquire a host of changes that are consistent with a predisposition to MDS and myeloid malignancies. For example, we see that expression of genes for key the epigenetic regulators *Dnmt3a* and *Ezh2* (both of which are found mutated in MDS and AML) are slightly but significantly downregulated with age. We also see that HSC-specific genes such as *Gata2* and *Hmga2* are hypomethylated and upregulated and that binding sites of TFs associated with differentiation, such as Pu.1, tend to become hypermethylated, whereas sites associated with factors involved in stem cell function (e.g., Scl) tend to be hypomethylated. Finally, we showed that the edges of DNA methylation canyons are highly dynamic in a manner concordant with loss of Dnmt3a function (Jeong et al., 2014; Challen et al., 2012), the mutation of which is associated with hematologic malignancies (Ley et al., 2010; Yan et al., 2011). Although our data cannot distinguish cause and effect with regard to these epigenetic changes with age, together they point to a stem cell state in which self-renewal is reinforced and differentiation is impeded—a cellular milieu likely to be conducive to transformation events.

Abating the Effects of Age

By using whole-genome analyses, we showed that concerted epigenetic changes may contribute to decreased differentiation and increased stem cell self-renewal. These data also show that the impact of epigenetic changes on aging is consistent, suggesting the possibility that some of the effects might be abated. Although aging is often regarded as an inexorable and irreversible process, emerging views suggests that the aging clock can be experimentally manipulated. Altogether, the findings here may allow the development of novel approaches to modulate HSC function.

EXPERIMENTAL PROCEDURES

Animals

C57BL/6 male mice were purchased from the National Institute for Aging and maintained at the Baylor College of Medicine Animal Care Facility under International Animal Care and Use Committee and institutional guidelines. None of the animals exhibited overt signs of pathology when sacrificed. We chose 24 months because this time point presages significant mortality increase and healthspan decline.

HSC Purification and Flow Cytometry

HSCs were purified from bone marrow of mice either 4 or 24 months of age. For all experiments, HSCs were purified as Hoechst SP-KLS and $CD150^{+}$ cells (see the Supplemental Experimental Procedures). Bone marrow cells were stained for 90 min with Hoechst, magnetically enriched for cells with c-expression, stained with additional antibodies, and then subjected to flow cytometric cell sorting. Purity was typically $\geq$ 95%.

RNA Sequencing

Batches of approximately 70,000 HSCs and 1 million B and Gr cells were sorted with fluorescence-activated cell sorting. RNA was isolated with the RNeasy Micro Kit (QIAGEN). Paired-end libraries were generated by with Illumina TruSeq RNA Sample Prep Kit. Illumina HiSeq was used for sequencing

density of canyons relative to aging DMCs. Density of peaks in 4mo HSCs at canyons subset by normalized counts of aging DMCs. H3K4me3 consists of H3K4me3 peaks alone. H3K27me3 consists of any peak region containing H3K27me3, including bivalent (co-occupancy by H3K4me3) and H3K27me3 alone. More Hypo and Hyper indicate canyons with greater numbers of hypomethylated or hypermethylated DMCs, respectively.
See also Figures S6 and S7.

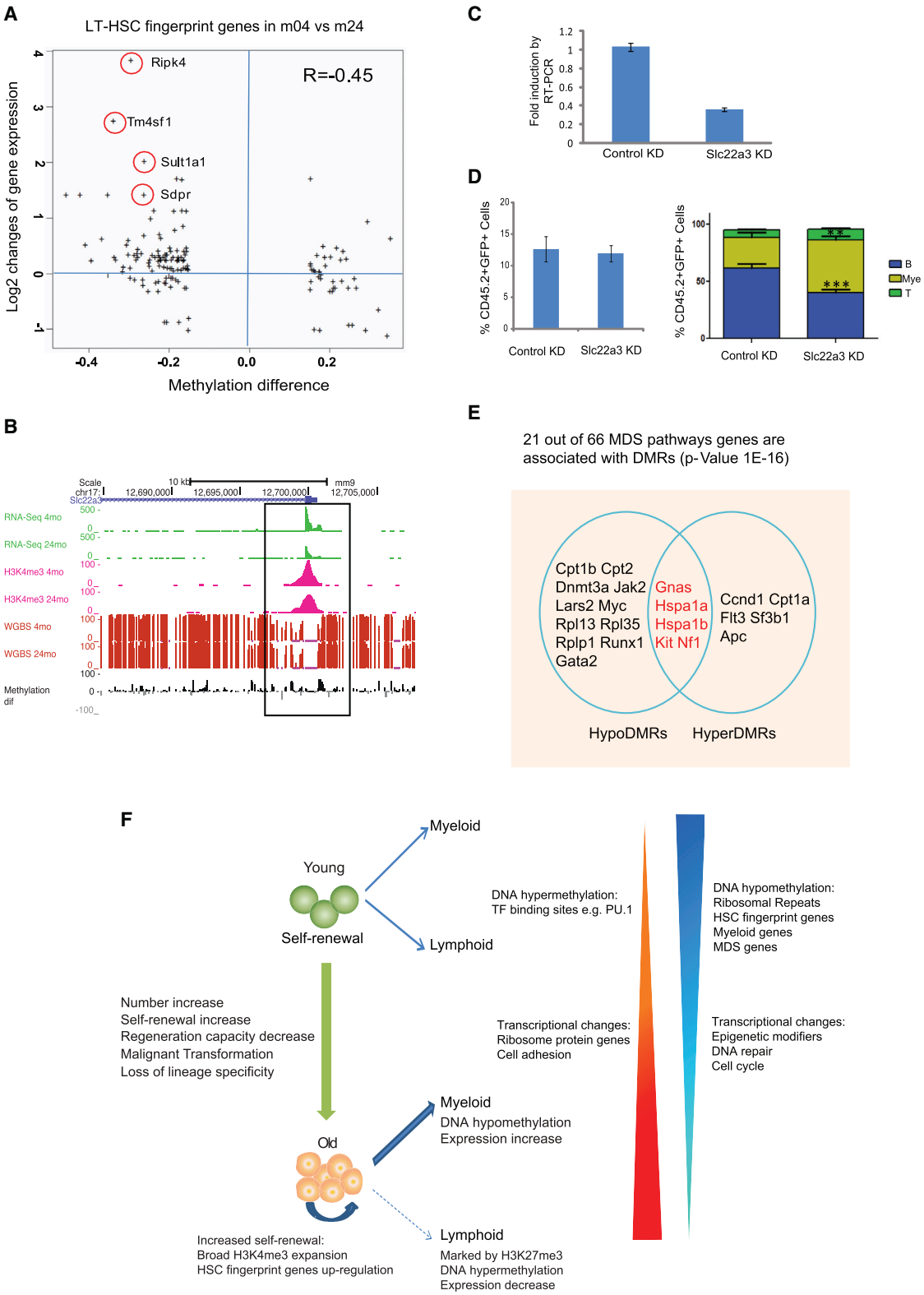

Figure 7. DNA Methylation Regulates HSC Function and Contributes to Age-Related Diseases

(A) The correlation between gene expression changes and methylation alterations for HSC fingerprint genes with DMRs. The x axis denotes the DMR methylation ratio difference, and the y axis denotes the log2 fold change of FPKM value for the gene. The circles mark the gene with names aside.

(legend continued on next page)

with a paired-end sequencing length of 100 bp. For analysis, the alignment was performed with the RNA-seq unified mapper, which first tries to map reads to genome and transcriptome by Bowtie, and then the reads unmapped to genome are handed to Blat for additional mapping. The information from the three mappings was merged into one mapping. Then, the multiplied mapped reads are discarded. The gene annotations used for transcriptome alignment include standard known-gene models (see the Supplemental Experimental Procedures). Differential expression was performed with DESeq. We used DAVID to examine these differentially expressed genes for functional enrichment in GO terms, KEGG Pathways, and SP_PIR_KEYWORDS. The unbiased gene-set enrichment analysis was performed with Gene Set Association Analysis sequencing (http://gsaa.unc.edu), which ranks all genes by DESeq differential test p values and examines enrichment of all gene sets in the Molecular Signatures Database and several manually created hematopoiesis fingerprint gene sets.

ChIP Sequencing

ChIP-seq was performed with 50,000 to 100,000 HSCs, B cells, and Gr cells (see the Supplemental Experimental Procedures). ChIP-seq DNA was made into sequencing libraries with ThruPLEX-FD (Rubicon). Sequencing was performed on an Illumina HiSeq 2000. The reads are mapped to mouse genome mm9 with SOAP2 by allowing at most two mismatches for 50 bp short reads and at most four mismatches for 100 bp short reads. Only uniquely mapped reads were retained. The reads from each biological replicate are fed as a treatment file into the model-based analysis of ChIP-seq data (MACS) program in order to find the peaks.

Whole-Genome Bisulfite Sequencing

300 ng genomic DNA was isolated from HSCs and fragmented with a Covaris sonication system (Covaris S2). Libraries were constructed with Illumina TruSeq DNA kit, ligated, and bisulfite-treated with the EpiTect Kit (QIAGEN). After determining the optimized PCR cycle number for each samples, a large-scale PCR reaction (100 μl) was performed (Gu et al., 2011). PCR products were sequenced with Illumina HiSeq sequencing systems. The WGBS data analyses were based on the model-based analysis of bisulfite sequencing (Sun et al., 2014) (http://code.google.com/p/moabs/).

Statistical and Bioinformatic Analysis

See the Supplemental Experimental Procedures.

ACCESSION NUMBERS

Data sets were deposited to the NCBI Gene Expression Omnibus under accession number GSE47819. Data and genome browser tracks can also be found at http://www.aginghscepigenome.us.

SUPPLEMENTAL INFORMATION

Supplemental Information contains Supplemental Experimental Procedures, seven figures, and seven tables and can be found with this article online at http://dx.doi.org/10.1016/j.stem.2014.03.002.

AUTHOR CONTRIBUTIONS

D.S., M.L., and M.J. designed and performed experiments; D.S., B.R., M.L., M.J., T.L., K.F.F., R.C., G.J.D., M.A.G., W.L., R.H., H.C., C.B., A.M., and B.G. analyzed the data; and D.S., M.L., B.R., M.J., T.L., K.F.F., B.G., M.A.G., W.L., and G.J.D. wrote and edited the manuscript.

ACKNOWLEDGMENTS

This work is dedicated to Estela Medrano. We thank Julio Hernandez for mouse management and Chris Threeton for flow cytometry. This work was supported by grants AG036562, AG288652, CA126752, DK092883, CA125123, DK084259, DK056338, AI07495, and AG000183 as well as the Ellison Medical Foundation, CPRIT grant RP110028, and the Samuel Waxman Cancer Research Foundation as well as HG007538, CPRIT RP110471, and DOD W81XWH-10-1-0501 to W.L. Support for T.L. came from T32 MH 19384-14, T32-HD007032, and the Eugene V. Cota-Robles Fellowship.

Received: July 17, 2013
Revised: December 16, 2013
Accepted: March 5, 2014
Published: May 1, 2014

REFERENCES

Beerman, I., Bhattacharya, D., Zandi, S., Sigvardsson, M., Weissman, I.L., Bryder, D., and Rossi, D.J. (2010). Functionally distinct hematopoietic stem cells modulate hematopoietic lineage potential during aging by a mechanism of clonal expansion. Proc. Natl. Acad. Sci. USA *107*, 5465–5470.

Beerman, I., Bock, C., Garrison, B.S., Smith, Z.D., Gu, H., Meissner, A., and Rossi, D.J. (2013). Proliferation-dependent alterations of the DNA methylation landscape underlie hematopoietic stem cell aging. Cell Stem Cell *12*, 413–425.

Bernstein, B.E., Mikkelsen, T.S., Xie, X., Kamal, M., Huebert, D.J., Cuff, J., Fry, B., Meissner, A., Wernig, M., Plath, K., et al. (2006). A bivalent chromatin structure marks key developmental genes in embryonic stem cells. Cell *125*, 315–326.

Blaney Davidson, E.N., Scharstuhl, A., Vitters, E.L., van der Kraan, P.M., and van den Berg, W.B. (2005). Reduced transforming growth factor-beta signaling in cartilage of old mice: role in impaired repair capacity. Arthritis Res. Ther. *7*, R1338–R1347.

Challen, G.A., Boles, N.C., Chambers, S.M., and Goodell, M.A. (2010). Distinct hematopoietic stem cell subtypes are differentially regulated by TGF-beta1. Cell Stem Cell *6*, 265–278.

Challen, G.A., Sun, D., Jeong, M., Luo, M., Jelinek, J., Berg, J.S., Bock, C., Vasanthakumar, A., Gu, H., Xi, Y., et al. (2012). Dnmt3a is essential for hematopoietic stem cell differentiation. Nat. Genet. *44*, 23–31.

Chambers, S.M., Boles, N.C., Lin, K.Y., Tierney, M.P., Bowman, T.V., Bradfute, S.B., Chen, A.J., Merchant, A.A., Sirin, O., Weksberg, D.C., et al. (2007a). Hematopoietic fingerprints: an expression database of stem cells and their progeny. Cell Stem Cell *1*, 578–591.

(B) University of Southern California browser track showing expression (green) and DNA methylation (red bars). Gray and black bars show differential methylation between 4mo and 24mo HSCs. H3K4me3 signal is shown in pink for the TSS region of *Slc22a3* in young and old HSCs.
(C) qRT-PCR to show that *Slc22a3* was knocked down by miRNA construct. Sca-1$^+$ cells were enriched from 5-fluorouracil-injected WT mice (4mo) and transduced with retroviral miRNA construct. After in vitro culture for 2 days, 20,000 GFP$^+$ cells were sorted for qRT-PCR. Error bars represent mean ± SEM. $^{**}p < 0.01$ and $^{***}p < 0.005$ (Student's t test).
(D) The left figure shows the contribution of retrovirally transduced donor HSCs (CD45.2$^+$GFP$^+$) to recipient mouse peripheral blood. Right figure shows the percentage of indicated lineages within the retrovirally transduced donor HSC-derived (CD45.2$^+$GFP$^+$) cell compartment in peripheral blood posttransplant (8 weeks). Myeloid cells (Mye) were defined with the markers Gr1$^+$ and Mac1$^+$, B cells (B) are B220$^+$ and T cells (T) are CD4$^+$ and CD8. n = 8 for each group. Error bars represent mean ± SEM. $^{**}p < 0.01$ and $^{***}p < 0.005$ (Student's t test).
(E) Venn diagram showing MDS genes with hyper- or hypo-DMRs. Regions with overlap have both hyper- and hypo-DMRs within same gene (distinct regions).
(F) Model for functional and epigenetic alterations with HSC aging. DNA hypomethylation in ribosomal repeats could initiate chromosomal instability and indicate HSC activation state. DNA hyper- or hypomethylation in master TF binding sites could contribute to reinforcement of self-renewal program and inhibition of differentiation.

Chambers, S.M., Shaw, C.A., Gatza, C., Fisk, C.J., Donehower, L.A., and Goodell, M.A. (2007b). Aging hematopoietic stem cells decline in function and exhibit epigenetic dysregulation. PLoS Biol. *5*, e201.

Cho, R.H., Sieburg, H.B., and Muller-Sieburg, C.E. (2008). A new mechanism for the aging of hematopoietic stem cells: aging changes the clonal composition of the stem cell compartment but not individual stem cells. Blood *111*, 5553–5561.

Cook, W.D., McCaw, B.J., Herring, C., John, D.L., Foote, S.J., Nutt, S.L., and Adams, J.M. (2004). PU.1 is a suppressor of myeloid leukemia, inactivated in mice by gene deletion and mutation of its DNA binding domain. Blood *104*, 3437–3444.

Curran, S.P., and Ruvkun, G. (2007). Lifespan regulation by evolutionarily conserved genes essential for viability. PLoS Genet. *3*, e56.

de Haan, G., and Van Zant, G. (1999). Dynamic changes in mouse hematopoietic stem cell numbers during aging. Blood *93*, 3294–3301.

Delhommeau, F., Dupont, S., Della Valle, V., James, C., Trannoy, S., Massé, A., Kosmider, O., Le Couedic, J.P., Robert, F., Alberdi, A., et al. (2009). Mutation in TET2 in myeloid cancers. N. Engl. J. Med. *360*, 2289–2301.

Dhayalan, A., Rajavelu, A., Rathert, P., Tamas, R., Jurkowska, R.Z., Ragozin, S., and Jeltsch, A. (2010). The Dnmt3a PWWP domain reads histone 3 lysine 36 trimethylation and guides DNA methylation. J. Biol. Chem. *285*, 26114–26120.

Dykstra, B., Olthof, S., Schreuder, J., Ritsema, M., and de Haan, G. (2011). Clonal analysis reveals multiple functional defects of aged murine hematopoietic stem cells. J. Exp. Med. *208*, 2691–2703.

Ergen, A.V., Boles, N.C., and Goodell, M.A. (2012). Rantes/Ccl5 influences hematopoietic stem cell subtypes and causes myeloid skewing. Blood *119*, 2500–2509.

Fan, X., Valdimarsdottir, G., Larsson, J., Brun, A., Magnusson, M., Jacobsen, S.E., ten Dijke, P., and Karlsson, S. (2002). Transient disruption of autocrine TGF-beta signaling leads to enhanced survival and proliferation potential in single primitive human hemopoietic progenitor cells. J. Immunol. *168*, 755–762.

Greer, E.L., Maures, T.J., Hauswirth, A.G., Green, E.M., Leeman, D.S., Maro, G.S., Han, S., Banko, M.R., Gozani, O., and Brunet, A. (2010). Members of the H3K4 trimethylation complex regulate lifespan in a germline-dependent manner in C. elegans. Nature *466*, 383–387.

Greer, E.L., Maures, T.J., Ucar, D., Hauswirth, A.G., Mancini, E., Lim, J.P., Benayoun, B.A., Shi, Y., and Brunet, A. (2011). Transgenerational epigenetic inheritance of longevity in Caenorhabditis elegans. Nature *479*, 365–371.

Grewal, S.S. (2009). Insulin/TOR signaling in growth and homeostasis: a view from the fly world. Int. J. Biochem. Cell Biol. *41*, 1006–1010.

Gründemann, D., Schechinger, B., Rappold, G.A., and Schömig, E. (1998). Molecular identification of the corticosterone-sensitive extraneuronal catecholamine transporter. Nat. Neurosci. *1*, 349–351.

Gu, H., Smith, Z.D., Bock, C., Boyle, P., Gnirke, A., and Meissner, A. (2011). Preparation of reduced representation bisulfite sequencing libraries for genome-scale DNA methylation profiling. Nat. Protoc. *6*, 468–481.

Hamilton, B., Dong, Y., Shindo, M., Liu, W., Odell, I., Ruvkun, G., and Lee, S.S. (2005). A systematic RNAi screen for longevity genes in C. elegans. Genes Dev. *19*, 1544–1555.

Hidalgo, I., Herrera-Merchan, A., Ligos, J.M., Carramolino, L., Nuñez, J., Martinez, F., Dominguez, O., Torres, M., and Gonzalez, S. (2012). Ezh1 is required for hematopoietic stem cell maintenance and prevents senescence-like cell cycle arrest. Cell Stem Cell *11*, 649–662.

Hodges, E., Molaro, A., Dos Santos, C.O., Thekkat, P., Song, Q., Uren, P.J., Park, J., Butler, J., Rafii, S., McCombie, W.R., et al. (2011). Directional DNA methylation changes and complex intermediate states accompany lineage specificity in the adult hematopoietic compartment. Mol. Cell *44*, 17–28.

Imamura, T., Takase, M., Nishihara, A., Oeda, E., Hanai, J., Kawabata, M., and Miyazono, K. (1997). Smad6 inhibits signalling by the TGF-beta superfamily. Nature *389*, 622–626.

Jacobsen, F.W., Stokke, T., and Jacobsen, S.E. (1995). Transforming growth factor-beta potently inhibits the viability-promoting activity of stem cell factor and other cytokines and induces apoptosis of primitive murine hematopoietic progenitor cells. Blood *86*, 2957–2966.

Jeong, M., Sun, D., Luo, M., Huang, Y., Challen, G.A., Rodriguez, B., Zhang, X., Chavez, L., Wang, H., Hannah, R., et al. (2014). Large conserved domains of low DNA methylation maintained by Dnmt3a. Nat. Genet. *46*, 17–23.

Kaeberlein, M., Powers, R.W., 3rd, Steffen, K.K., Westman, E.A., Hu, D., Dang, N., Kerr, E.O., Kirkland, K.T., Fields, S., and Kennedy, B.K. (2005). Regulation of yeast replicative life span by TOR and Sch9 in response to nutrients. Science *310*, 1193–1196.

Kamminga, L.M., Bystrykh, L.V., de Boer, A., Houwer, S., Douma, J., Weersing, E., Dontje, B., and de Haan, G. (2006). The Polycomb group gene Ezh2 prevents hematopoietic stem cell exhaustion. Blood *107*, 2170–2179.

Ko, M., Bandukwala, H.S., An, J., Lamperti, E.D., Thompson, E.C., Hastie, R., Tsangaratou, A., Rajewsky, K., Koralov, S.B., and Rao, A. (2011). Ten-Eleven-Translocation 2 (TET2) negatively regulates homeostasis and differentiation of hematopoietic stem cells in mice. Proc. Natl. Acad. Sci. USA *108*, 14566–14571.

Langemeijer, S.M., Kuiper, R.P., Berends, M., Knops, R., Aslanyan, M.G., Massop, M., Stevens-Linders, E., van Hoogen, P., van Kessel, A.G., Raymakers, R.A., et al. (2009). Acquired mutations in TET2 are common in myelodysplastic syndromes. Nat. Genet. *41*, 838–842.

Ley, T.J., Ding, L., Walter, M.J., McLellan, M.D., Lamprecht, T., Larson, D.E., Kandoth, C., Payton, J.E., Baty, J., Welch, J., et al. (2010). DNMT3A mutations in acute myeloid leukemia. N. Engl. J. Med. *363*, 2424–2433.

Li, Z., Cai, X., Cai, C.L., Wang, J., Zhang, W., Petersen, B.E., Yang, F.C., and Xu, M. (2011). Deletion of Tet2 in mice leads to dysregulated hematopoietic stem cells and subsequent development of myeloid malignancies. Blood *118*, 4509–4518.

Linton, P.J., and Dorshkind, K. (2004). Age-related changes in lymphocyte development and function. Nat. Immunol. *5*, 133–139.

Liu, L., Cheung, T.H., Charville, G.W., Hurgo, B.M., Leavitt, T., Shih, J., Brunet, A., and Rando, T.A. (2013). Chromatin modifications as determinants of muscle stem cell quiescence and chronological aging. Cell Rep *4*, 189–204.

Loffredo, F.S., Steinhauser, M.L., Jay, S.M., Gannon, J., Pancoast, J.R., Yalamanchi, P., Sinha, M., Dall'Osso, C., Khong, D., Shadrach, J.L., et al. (2013). Growth differentiation factor 11 is a circulating factor that reverses age-related cardiac hypertrophy. Cell *153*, 828–839.

López-Otín, C., Blasco, M.A., Partridge, L., Serrano, M., and Kroemer, G. (2013). The hallmarks of aging. Cell *153*, 1194–1217.

Maegawa, S., Hinkal, G., Kim, H.S., Shen, L., Zhang, L., Zhang, J., Zhang, N., Liang, S., Donehower, L.A., and Issa, J.P. (2010). Widespread and tissue specific age-related DNA methylation changes in mice. Genome Res. *20*, 332–340.

Mayle, A., Luo, M., Jeong, M., and Goodell, M.A. (2013). Flow cytometry analysis of murine hematopoietic stem cells. Cytometry A *83*, 27–37.

Meissner, A., Mikkelsen, T.S., Gu, H., Wernig, M., Hanna, J., Sivachenko, A., Zhang, X., Bernstein, B.E., Nusbaum, C., Jaffe, D.B., et al. (2008). Genome-scale DNA methylation maps of pluripotent and differentiated cells. Nature *454*, 766–770.

Min, I.M., Pietramaggiori, G., Kim, F.S., Passegué, E., Stevenson, K.E., and Wagers, A.J. (2008). The transcription factor EGR1 controls both the proliferation and localization of hematopoietic stem cells. Cell Stem Cell *2*, 380–391.

Molofsky, A.V., Slutsky, S.G., Joseph, N.M., He, S., Pardal, R., Krishnamurthy, J., Sharpless, N.E., and Morrison, S.J. (2006). Increasing p16INK4a expression decreases forebrain progenitors and neurogenesis during ageing. Nature *443*, 448–452.

Moran-Crusio, K., Reavie, L., Shih, A., Abdel-Wahab, O., Ndiaye-Lobry, D., Lobry, C., Figueroa, M.E., Vasanthakumar, A., Patel, J., Zhao, X., et al. (2011). Tet2 loss leads to increased hematopoietic stem cell self-renewal and myeloid transformation. Cancer Cell *20*, 11–24.

Morrison, S.J., Wandycz, A.M., Akashi, K., Globerson, A., and Weissman, I.L. (1996). The aging of hematopoietic stem cells. Nat. Med. *2*, 1011–1016.

Narla, A., and Ebert, B.L. (2010). Ribosomopathies: human disorders of ribosome dysfunction. Blood *115*, 3196–3205.

Pan, K.Z., Palter, J.E., Rogers, A.N., Olsen, A., Chen, D., Lithgow, G.J., and Kapahi, P. (2007). Inhibition of mRNA translation extends lifespan in Caenorhabditis elegans. Aging Cell *6*, 111–119.

Papaemmanuil, E., Cazzola, M., Boultwood, J., Malcovati, L., Vyas, P., Bowen, D., Pellagatti, A., Wainscoat, J.S., Hellstrom-Lindberg, E., Gambacorti-Passerini, C., et al.; Chronic Myeloid Disorders Working Group of the International Cancer Genome Consortium (2011). Somatic SF3B1 mutation in myelodysplasia with ring sideroblasts. N. Engl. J. Med. *365*, 1384–1395.

Quivoron, C., Couronné, L., Della Valle, V., Lopez, C.K., Plo, I., Wagner-Ballon, O., Do Cruzeiro, M., Delhommeau, F., Arnulf, B., Stern, M.H., et al. (2011). TET2 inactivation results in pleiotropic hematopoietic abnormalities in mouse and is a recurrent event during human lymphomagenesis. Cancer Cell *20*, 25–38.

Ramos-Casals, M., García-Carrasco, M., Brito, M.P., López-Soto, A., and Font, J. (2003). Autoimmunity and geriatrics: clinical significance of autoimmune manifestations in the elderly. Lupus *12*, 341–355.

Rossi, D.J., Bryder, D., Zahn, J.M., Ahlenius, H., Sonu, R., Wagers, A.J., and Weissman, I.L. (2005). Cell intrinsic alterations underlie hematopoietic stem cell aging. Proc. Natl. Acad. Sci. USA *102*, 9194–9199.

Sirin, O., Lukov, G.L., Mao, R., Conneely, O.M., and Goodell, M.A. (2010). The orphan nuclear receptor Nurr1 restricts the proliferation of haematopoietic stem cells. Nat. Cell Biol. *12*, 1213–1219.

Stadler, M.B., Murr, R., Burger, L., Ivanek, R., Lienert, F., Schöler, A., van Nimwegen, E., Wirbelauer, C., Oakeley, E.J., Gaidatzis, D., et al. (2011). DNA-binding factors shape the mouse methylome at distal regulatory regions. Nature *480*, 490–495.

Sun, D., Xi, Y., Rodriguez, B., Park, H.J., Tong, P., Meong, M., Goodell, M.A., and Li, W. (2014). MOABS: model based analysis of bisulfite sequencing data. Genome Biol. *15*, R38.

Syntichaki, P., Troulinaki, K., and Tavernarakis, N. (2007). eIF4E function in somatic cells modulates ageing in Caenorhabditis elegans. Nature *445*, 922–926.

Venezia, T.A., Merchant, A.A., Ramos, C.A., Whitehouse, N.L., Young, A.S., Shaw, C.A., and Goodell, M.A. (2004). Molecular signatures of proliferation and quiescence in hematopoietic stem cells. PLoS Biol. *2*, e301.

Villeda, S.A., Luo, J., Mosher, K.I., Zou, B., Britschgi, M., Bieri, G., Stan, T.M., Fainberg, N., Ding, Z., Eggel, A., et al. (2011). The ageing systemic milieu negatively regulates neurogenesis and cognitive function. Nature *477*, 90–94.

Wang, J., Sun, Q., Morita, Y., Jiang, H., Gross, A., Lechel, A., Hildner, K., Guachalla, L.M., Gompf, A., Hartmann, D., et al. (2012). A differentiation checkpoint limits hematopoietic stem cell self-renewal in response to DNA damage. Cell *148*, 1001–1014.

Weishaupt, H., Sigvardsson, M., and Attema, J.L. (2010). Epigenetic chromatin states uniquely define the developmental plasticity of murine hematopoietic stem cells. Blood *115*, 247–256.

Wilson, N.K., Foster, S.D., Wang, X., Knezevic, K., Schütte, J., Kaimakis, P., Chilarska, P.M., Kinston, S., Ouwehand, W.H., Dzierzak, E., et al. (2010). Combinatorial transcriptional control in blood stem/progenitor cells: genome-wide analysis of ten major transcriptional regulators. Cell Stem Cell *7*, 532–544.

Xie, W., Schultz, M.D., Lister, R., Hou, Z., Rajagopal, N., Ray, P., Whitaker, J.W., Tian, S., Hawkins, R.D., Leung, D., et al. (2013). Epigenomic analysis of multilineage differentiation of human embryonic stem cells. Cell *153*, 1134–1148.

Yan, X.J., Xu, J., Gu, Z.H., Pan, C.M., Lu, G., Shen, Y., Shi, J.Y., Zhu, Y.M., Tang, L., Zhang, X.W., et al. (2011). Exome sequencing identifies somatic mutations of DNA methyltransferase gene DNMT3A in acute monocytic leukemia. Nat. Genet. *43*, 309–315.

Yu, Q., and Stamenkovic, I. (2000). Cell surface-localized matrix metalloproteinase-9 proteolytically activates TGF-beta and promotes tumor invasion and angiogenesis. Genes Dev. *14*, 163–176.

Ziller, M.J., Gu, H., Müller, F., Donaghey, J., Tsai, L.T., Kohlbacher, O., De Jager, P.L., Rosen, E.D., Bennett, D.A., Bernstein, B.E., et al. (2013). Charting a dynamic DNA methylation landscape of the human genome. Nature *500*, 477–481.